Article

Entropy-Driven Thermo-gelling Vitrimer

Xiuyang Xia, Peilin Rao, Juan Yang, Massimo Pica Ciamarra, and Ran Ni*

Read Online

ACCESS | Metrics & More | Article Recommendations | Supporting Information

ABSTRACT: Thermo-gelling polymers have been envisioned as promising smart biomaterials but limited by their weak mechanical and thermodynamic stabilities. Here, we propose a new thermo-gelling vitrimer, which remains at a liquid state because of the addition of protector molecules preventing the crosslinking, and with increasing temperature, an entropy-driven crosslinking occurs to induce the sol−gel transition. Moreover, we find that the activation barrier in the metathesis reaction of vitrimers plays an important role, and experimentally, one can use catalysts to tune the activation barrier to drive the vitrimer to form an equilibrium gel at high temperature, which is not subject to any thermodynamic instability. We formulate a mean-field theory to describe the entropy-driven crosslinking of the vitrimer, which agrees quantitatively with computer simulations and paves the way for the design and fabrication of novel vitrimers for biomedical applications.

KEYWORDS: *vitrimer, entropy-driven crosslinking, thermo-gelling elastomer, equilibrium gel, mean-field theory, computer simulation*
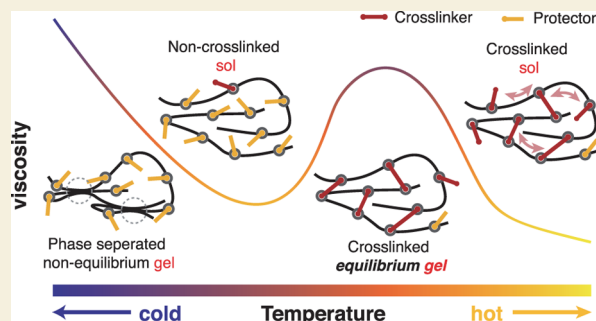
INTRODUCTION

Thermo-gels are polymers that undergo a sol−gel transition with increasing temperature. Over the past decades, thermo-gels have gained extensive attention in biomaterials and biomedical sciences,[1−4] because of their significant potential in applications of shape-memory polymer,[5] drug delivery,[6−8] tissue engineering,[9] bioseparations,[10,11] and so forth. The typical mechanism of thermo-gelling involves noncovalent interactions in the material such as hydrogen bonding,[12] Coulombic,[13] and competing van der Waals interactions.[14] By increasing temperature, the intra- and intermolecular interactions outbalance the solvent effect, thereby resulting in the gelation of the material.[15−17] However, the weak noncovalent interaction usually leads to low mechanical stability and rapid disintegrations in physiological environments.[18,19] To overcome those challenges, one may obtain permanently cross-linked gel networks with higher mechanical stability by using chemical reactions such as Michael addition,[20] enzymatic crosslinking,[21,22] or photo-induced crosslinking.[18,23] However, the gel formation requires an extra reprocessing step that is difficult to control or not applicable for thick or opaque samples,[24−26] and the formed gel would lose the reversibility.

Vitrimers are a unique type of crosslinked polymer network with dynamic and exchangeable covalent bonds.[27] They have shown great promise as recyclable materials in chemical and materials industries. The exchangeability originates from the reversible reactions between polymer backbones and small crosslinkers through metathesis reactions. The rate of these reactions is governed by temperature, and some of them, for example, silyl ether metathesis,[28] thio-disulfide exchange

reaction, and[29,30] dynamic Schiff base,[31,32] are biocompatible and applicable *in vivo*. In this work, based on a recently developed linker-mediated vitrimer using metathesis reactions,[33,34] we propose a new reversible thermo-gelling polymer. The polymer remains as an uncrosslinked liquid at low temperatures and solidifies to a covalently crosslinked elastomer with increasing temperature. To describe the crosslinking of the designed thermo-gelling vitrimer, we formulate a mean-field theory, which quantitatively agrees with coarse-grained computer simulations. Moreover, we find that the activation barrier of metathesis reactions plays a crucial role in driving the formation of an equilibrium gel with increasing temperature.

MODEL AND MEAN FIELD THEORY

We consider a system of volume V consisting of N_{poly} polymer chains, and each polymer chain comprises n connected hard spheres of diameter σ as the backbone, on which m precursors P are uniformly distributed. As shown in Figure 1a,c, each P can react with a cross-linker molecule C or a protector molecule D to form a dangling PC or PD bond through metathesis reactions of reaction free energy $\Delta G_C = -\varepsilon$ or ΔG_D
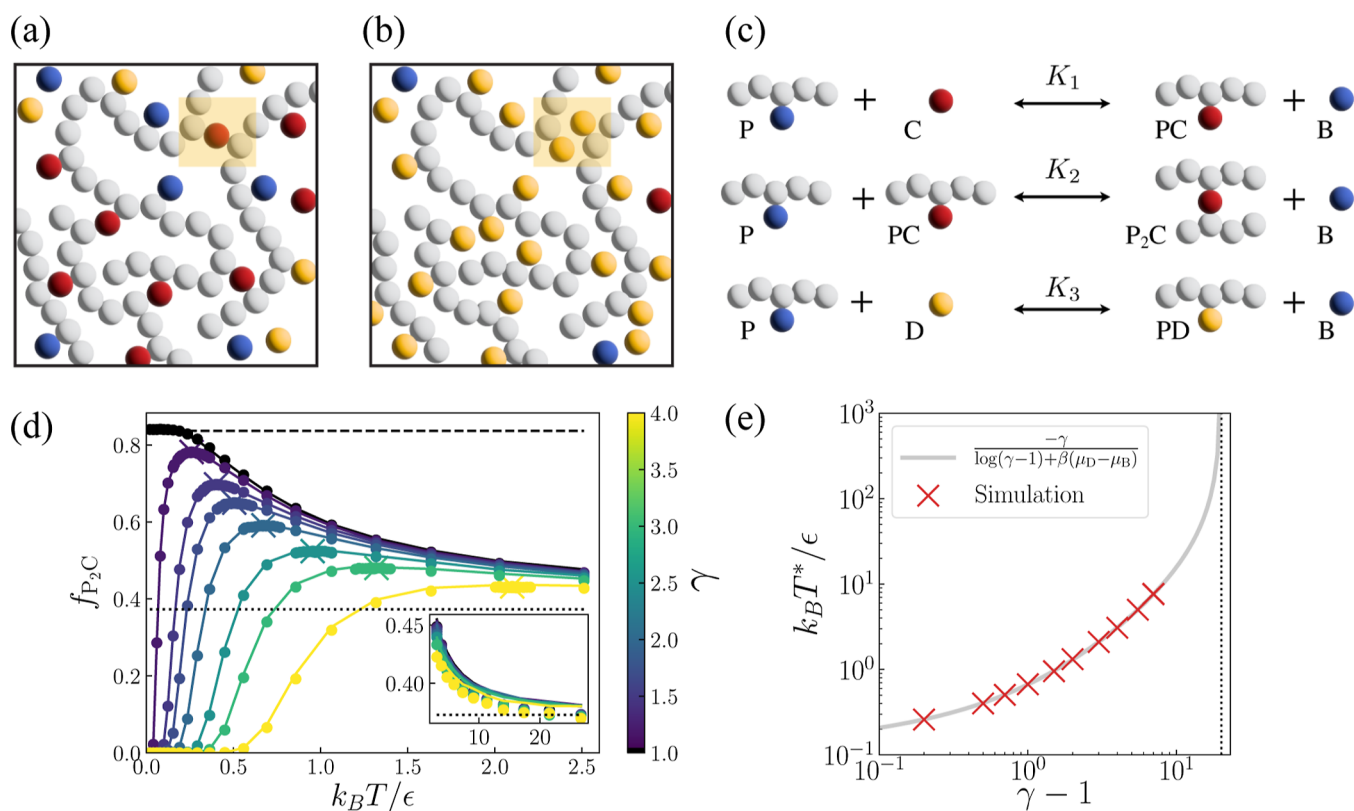
Figure 1. Entropy-driven crosslinking vitrimers. (a) Schematic representation of the linker-mediated vitrimer protected by small protector molecule D. (b) At low temperature, PD bonds dominate the system with no crosslinking formed. The rectangular yellow region indicates that a P_2C crosslinking bond transforms into two dangling PD bonds at low temperatures. (c) Three metathesis reactions in the linker-mediated vitrimer, of which the reaction constants are K_1, K_2, and K_3, respectively. (d) The crosslinking degree f_{P_2C} as a function of temperature $k_B T/\epsilon$ for various γ from 1.0 to 4.0. Symbols are values obtained from simulations and solid lines are the theoretical prediction of eq 6 using K_2/K_1 calculated from simulations. The dotted and dashed horizontal lines are the values of f_{P_2C} at the high-temperature limit and at the low-temperature limit with $\gamma = 1$ theoretically predicted by eq 6 with eqs 12 and 14, respectively. × symbols indicate the location of the maximum value of f_{P_2C} obtained in simulations. Inset: f_{P_2C} as a function of $k_B T/\epsilon$ with at higher temperature showing the convergence to the theoretical prediction. (e) Optimal temperature $k_B T*/\epsilon$ as a function of γ, where symbols are from simulations, and the grey curve is the theoretical prediction of eq 15. The dotted vertical line shows the critical γ where $T*$ diverges. Here $N_{poly} = 100$, $\phi_p = 0.25$, $\chi_{att} = 0$, $\beta\mu_B = -2$, $\beta\mu_C = -4$, and $\beta\mu_D = -5$.

$= -\gamma\epsilon$, respectively, by releasing a byproduct molecule B. Only dangling PC bonds can further react with another precursor P to form a P_2C crosslinking bond through the same metathesis reaction. To ensure no crosslinking formed at the low-temperature limit (as shown in Figure 1b), we consider $\gamma > 1$. Small molecules B, C, and D are modeled as hard spheres of diameter σ and controlled by the chemical potential μ_B, μ_C, and μ_D, respectively. We assume that densities of small molecules in the reservoir remain constant for all temperatures, that is, $\beta\mu_B$, $\beta\mu_C$, and $\beta\mu_D$ do not change with T. Here $\beta = 1/k_B T$ with k_B and T the Boltzmann constant and temperature of the system, respectively. The packing fraction of polymer backbones is $\phi_p = \pi N_{poly} n\sigma^3/6V$, and N_i is the number of bonds or molecules in the system, where i = P, PC, PD, P_2C, B, C, and D. An infinitely deep square-well potential is employed to mimic the covalent bonds in the system

$$V_{bond}(\boldsymbol{r}, \boldsymbol{r}') = \begin{cases} 0 & |\boldsymbol{r} - \boldsymbol{r}'| < r_{bond} \\ \infty & \text{else} \end{cases} \quad (1)$$

where r_{bond} is the cut-off distance of the covalent bond. We use the square-well potential to model the van der Waals short-range attraction between polymer backbones

$$V_{att}(\boldsymbol{r}, \boldsymbol{r}') = \begin{cases} -\chi_{att}\epsilon & |\boldsymbol{r} - \boldsymbol{r}'| < r_{att} \\ 0 & \text{else} \end{cases} \quad (2)$$

where χ_{att} and r_{att} are the strength and interaction range of the attraction, respectively. To be experimentally relevant, we choose $n = 100$, $m = 8$, and $r_{bond} = r_{att} = 1.5\sigma$ throughout all simulations in this work.

The free energy of the system can be written as

$$\beta F = \sum_{i=poly,B,C,D} N_i \left[\ln\left(\frac{N_i \Lambda^3}{V}\right) - 1 \right] + \sum_{i=P,PC,PD,P_2C} N_i$$
$$\times \left[\ln\left(\frac{n_i \Lambda^3}{V_p}\right) - 1 \right] - N_{P_2C} k_B^{-1} \Delta S + \beta F_{att} + \beta F_{HS}^{ex} - \beta N_B \mu_B$$
$$- \beta(N_{PC} + N_{P_2C} + N_C)\mu_C - \beta(N_{PD} + N_D)\mu_D$$
$$+ \beta(N_{PC} + 2N_{P_2C})(\Delta G_C + \mu_B) + \beta N_{PD}(\Delta G_D + \mu_B)$$
$$(3)$$

where Λ is the de Broglie wavelength. The first summation is on the ideal gas in terms of polymer blobs (poly), byproduct molecules (B), free crosslinkers (C), and protectors (D). The second summation is on the ideal gas terms of precursors P,

PC bonds, PD bonds, and P_2C bonds on a polymer confined within the volume V_p, which can be seen as the volume occupied by a polymer, and $n_i = N_i/N_{poly}$ is the number of bonds per polymer with i = P, PC, PD, P_2C. ΔS accounts for the entropy change of the system by forming a P_2C crosslinking bond, and F_{att} is the free energy contribution from the van der Waals short-range attraction between polymer backbones. It is known that the structure of a homogeneous fluid is mainly determined by the repulsion between molecules.[35] Therefore, $F_{att} \approx -\chi_{att}\varepsilon g(\phi)$, and $g(\phi)$ is a function of the total packing fraction of the system ϕ, which can be seen as the total number of nonbonded attractive pairs of backbone beads formed in the system. F_{HS}^{ex} is the excess free energy accounting for the crowding effect, which we approximate with the Carnahan–Starling hard-sphere equation of state[36] (see Supporting Information S1), and it depends on the total packing fraction of the system ϕ. The other five terms arise from the bond swaps in metathesis reactions related to ΔG_C and ΔG_D, and the exchange of molecules with reservoir related to μ_B, μ_C, and μ_D.

We define the crosslinking degree of the system as $f_{P_2C} = 2N_{P_2C}/(N_{poly}m)$ and the fraction of other bonds or molecules as $f_i = N_i/(N_{poly}m)$ where i = P, PD, PC, B, C, D, and

$$f_P + f_{PC} + f_{PD} + f_{P_2C} = 1 \tag{4}$$

With the saddle point approximation, that is, $\partial F/\partial\{f_j\} = 0$ with j = PC, PD, P_2C, we have $f_{PC} = f_P\Xi_{PC}$, $f_{PD} = f_P\Xi_{PD}$ and $f_{P_2C} = f_P{}^2\Xi_{P_2C}$, where

$$\Xi_{P_2C} = (2m\Lambda^3/V_p)\exp[\beta(\mu_C - 2\mu_B + 2\varepsilon + \mu_{HS}^{ex}) + k_B^{-1}\Delta S]$$

$$\Xi_{PC} = \exp[\beta(\mu_C - \mu_B + \varepsilon)]$$

$$\Xi_{PD} = \exp[\beta(\mu_D - \mu_B + \gamma\varepsilon)] \tag{5}$$

μ_{HS}^{ex} is the excess free energy of hard spheres with packing fraction ϕ, which can be calculated by self-consistent iterations (see Supporting Information S1). Here we note that $\partial F_{att}/\partial f_j \approx -\chi_{att}\varepsilon(\partial g/\partial\phi)(\partial\phi/\partial f_j) \approx 0$, with the assumption that the system is mainly composed of polymer backbones, and the metathesis reactions have minor effects on the packing fraction of the system, that is, $\partial\phi/\partial f_j \approx 0$. Substituting these terms into eq 4, we obtain

$$f_{P_2C} = (\sqrt{\Gamma^2 + 1} - \Gamma)^2 \tag{6}$$

where

$$\Gamma = \frac{1 + \Xi_{PC} + \Xi_{PD}}{2\sqrt{\Xi_{P_2C}}} \tag{7}$$

Moreover, V_p and ΔS can be obtained by considering the chemical and reaction equilibrium (see Supporting Information S2)

$$\frac{K_2}{K_1} = \frac{V}{N_{poly}V_p}e^{\Delta S/k_B} \tag{8}$$

where K_1 and K_2 are reaction constants of the first two metathesis reactions in Figure 1c and can be measured directly in computer simulations.

SIMULATIONS

Monte Carlo Simulation

We perform Monte Carlo (MC) simulations to investigate the equilibrium properties of the thermo-crosslinking vitrimer. Assuming the bulk density conservation of B, C, and D when temperature varies, we employed grand canonical $\beta\mu_B\mu_C\mu_D$–$N_{poly}VT$ MC simulations to simulate the coarse-grained hard-sphere-chain system, with the temperature unit ε/k_B. Simulations are performed with N_{poly} polymer chains with n beads per chain, where periodic boundary conditions are applied in all three dimensions with the cubic box volume $V = \pi/6N_{poly}n/\phi_p$. The translational moves of particles are implemented by the straight event-chain algorithm,[37,38] in which the length of each event is fixed at $L_c = 10\sigma$, and the pressure P of the system can be calculated by the mean excess chain displacement

$$P = k_BT\rho\left\langle\frac{x_{final} - x_{initial}}{L_c}\right\rangle_{chains} \tag{9}$$

where $x_{initial}$ and x_{final} are the projection of initial and final particle positions on the chain direction of each event chain, ρ is the number density of the particles, and $\langle\cdot\rangle_{chains}$ calculates the average overall event chains. Molecules B, C, and D are inserted or removed using the conventional grand canonical MC method. Besides, we devise a simple bond swap algorithm to simulate reversible bond swap metathesis reactions in the vitrimer system (see below), respecting the detailed balance. The ratio of three types of trial moves, translational moves, inserting/removing molecules, and bond swaps, is 1:4:5. In each simulation, we perform 10^9 MC moves for equilibration and 10^9 MC moves for sampling.

Hybrid Event-Driven Molecular Dynamics—Monte Carlo Simulation

We perform the hybrid event-driven molecular dynamics—Monte Carlo (EDMD–MC) simulation[39−41] to measure the intermediate scattering function $F_s(q, t)$ and the structural relaxation time τ_α in the canonical (NVT) ensemble starting from equilibrated configurations from our grand canonical MC simulations; as in EDMD, it is not efficient to vary the number of molecules. All the bond swaps in metathesis reactions are done by the MC algorithm below.[42] In our simulations, $N_{poly}m$ bond swap attempts are performed per time interval τ_{MD}. Each simulation consists of $10^6\tau_{MD}$ for equilibration and $10^6\tau_{MD}$ for sampling. An Anderson thermostat[42,43] is applied to all molecules every $\tau_{ads} = 0.005\tau_{MD}$ to control the temperature of the system, and we ensure that further decreasing τ_{ads} does not change any simulation results. Here $\tau_{MD} = (m_b\sigma^2/\varepsilon)^{1/2}$ is the time unit of MD simulations, and m_b is the mass of a polymer bead, where we assume all the small molecules, that is, B, C, and D, to have the same mass as a polymer bead. The self-intermediate scattering function $F_s(q, t)$ with wave vector q and time t is a common indicator for structural relaxation in MD simulations[39]

$$F_s(q, t) = \frac{1}{nN_{poly}}\left\langle\sum_{j=1}^{nN_{poly}}\exp[i\mathbf{q}\cdot(\mathbf{r}_j(t) - \mathbf{r}_j(0))]\right\rangle \tag{10}$$

which calculates overall backbone beads with position $\mathbf{r}$ on the vitrimers.

Bond Swap Algorithm

In our MC simulations, a typical reversible single bond−swap reaction is
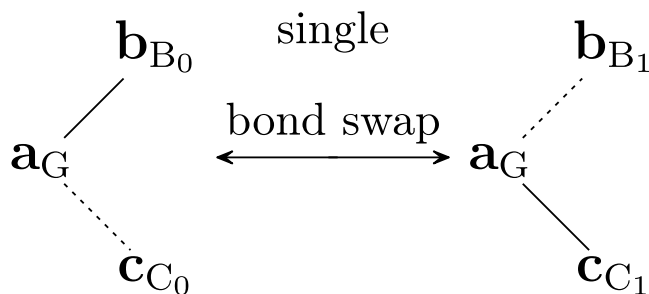
where $\mathbf{a}/\mathbf{b}/\mathbf{c}$ and $G/A_0/A_1/B_0/B_1$ are the specific beads/particles and types as shown in the three kinds of reactions in Figure 1c. G is the type of polymer backbone beads grafted by precursors initially. The proposed move for the forward reaction can be constructed by the following two steps:

1. Choose a *pivot* particle $\mathbf{a}$ (type G) bounded with $\mathbf{b}$ (type B_0 = P, PC, P_2C or PD) with probability $p(\mathbf{a})$. Note there is precisely one bond that can be swapped for each pivot particle;

2. Choose a neighboring potentially reactive particle $\mathbf{c}$ (type C_0 = B, C, D, or PC) within the distance r_{bond} randomly with probability $h(\mathbf{c}_{C_0}|\mathbf{a})$;

One can see the above bond swap move does not change the number of neighbor potentially reactive particles and bonds of $\mathbf{a}$; hence, both before and after a bond swap move $h(\mathbf{c}_{C_0}|\mathbf{a}) = h(\mathbf{b}_{B_1}|\mathbf{a})$. For the first and third reactions, shown in Figure 1c, the acceptance probability of the proposed move of the forward and backward reactions are $\exp(-\beta\Delta G)$ and $\exp(\beta\Delta G)$, respectively, with the free energy of the forward reaction being ΔG. For the second reaction in Figure 1c, we double the forward reaction flux to equalize the flux between the two states before and after the reaction.[34]

Furthermore, for mimicking the actual topology and reaction dynamics of vitrimers, that is, the covalent bond-exchange dynamics in Figure S3, we perform additional double bond swap reactions in the EDMD-MC simulation as follows, before and after which no chemical potential change in the system:
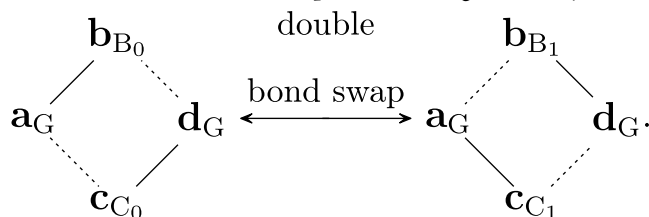
We randomly choose each specific bond swap move in three steps:

1. Select a *pivot* particle $\mathbf{a}$ (type G) bounded with $\mathbf{b}$ (type B_0 = P, PC, P_2C, or PD) with probability $p(\mathbf{a})$;

2. Select a neighboring potentially reactive particle $\mathbf{c}$ other than $\mathbf{b}$ (type C_0 = B, C, D, PB, PC, P_2C, or PD) within a random distance r_{bond} with probability $h(\mathbf{c}_{C_0}|\mathbf{a})$.

3. Select a reaction type (single bond/double bond) with probability $g(\mathbf{c}_{C_0}|\mathbf{b}_{B_0})$.

Similarly, here $h(\mathbf{c}_{C_0}|\mathbf{a}) = h(\mathbf{b}_{B_1}|\mathbf{a})$. g accounts for the number of possible bonds combinations, and if $\mathbf{b}_{B_0}/\mathbf{c}_{C_0}$ can undergo both single-bond swap and double-bond swap, $g(\mathbf{c}_{C_0}|\mathbf{b}_{B_0}) = 0.5$, otherwise, $g(\mathbf{c}_{C_0}|\mathbf{b}_{B_0}) = 1$. Additionally, we consider that all metathesis reactions share the same activation barrier, ΔG_b, and activation free energy, $\Delta G_b + \max(\Delta G, 0)$. A bond swap attempt first needs to overcome the energy barrier with probability, $\mathrm{acc}_b = \exp(-\Delta G_b/k_BT)$, and then is accepted with the probability

$$\mathrm{acc}_r = \min\left[1, \frac{g(\mathbf{b}_{b_0}|\mathbf{a}_{a_0})}{g(\mathbf{a}_{a_1}|\mathbf{b}_{b_1})}\exp(-\beta\Delta G)\right] \tag{11}$$

where ΔG is the bond swap reaction free energy.

■ RESULTS

Entropy-Driven Crosslinking

First, we investigate the crosslinking in the system without any short-range van der Waals attraction, that is, $\chi_{att} = 0$, and in Figure 1d we plot the calculated f_{P_2C} from Monte Carlo (MC) simulations for various γ as functions of temperature k_BT/ε in comparison with the theoretical prediction of eq 6, in which the only input from simulations is K_2/K_1. One can see that the results from computer simulation quantitatively agree with the mean-field theory. At $\gamma = 1$, f_{P_2C} reaches two different positive plateaus at $T \to 0$ and $T \to \infty$, respectively, with $f_{P_2C}(T \to 0) > f_{P_2C}(T \to \infty)$. When $\gamma > 1$, as shown in Figure 1d, $f_{P_2C}(T \to 0) \to 0$, and with increasing temperature, f_{P_2C} increases to reach a maximum at temperature T^* then decreases to approach the same plateau at high temperatures, which does not depend on γ. These can be understood as follows. At the high-temperature limit, $\beta\varepsilon \to 0$, the crosslinking in the system is solely determined by entropy, and

$$\Gamma^\infty = \frac{1 + \Xi_{PC}^\infty + \Xi_{PD}^\infty}{2\sqrt{\Xi_{P_2C}^\infty}} \tag{12}$$

where

$$\Xi_{PC}^\infty = \exp[\beta(\mu_C - \mu_B)]$$

$$\Xi_{PD}^\infty = \exp[\beta(\mu_D - \mu_B)]$$

$$\Xi_{P_2C}^\infty = (2m\Lambda^3/V_p)\exp[\beta(\mu_C - 2\mu_B + \mu_{HS}^{ex}) + k_B^{-1}\Delta S] \tag{13}$$

which does not depend on γ. This can be further used to calculate $f_{P_2C}^\infty$ using eq 6. Moreover, at the low-temperature limit, that is, $\beta\varepsilon \to \infty$, when $\gamma = 1$, the saddle-point solution of Γ can be obtained by the Lagrange multiplier method (see Supporting Information S4)

$$\Gamma^0 = \frac{\Xi_{PC}^\infty + \Xi_{PD}^\infty}{2\sqrt{\Xi_{P_2C}^\infty}} \tag{14}$$

with which we can calculate the low-temperature plateau $f_{P_2C}^0$ for $\gamma = 1$ with eq 6. One can see that $\Gamma^\infty > \Gamma^0$, which implies $f_{P_2C}^\infty < f_{P_2C}^0$, as eq 6 is a monotonically decreasing function of Γ. When $\gamma > 1$, as the formation of PD bonds is more energetically favorable than that of PC bonds, the crosslinking is prevented at the low-temperature limit, and at small γ, the competition between entropy-driven crosslinking and enthalpy-driven protection by PD bonds leads to the non-
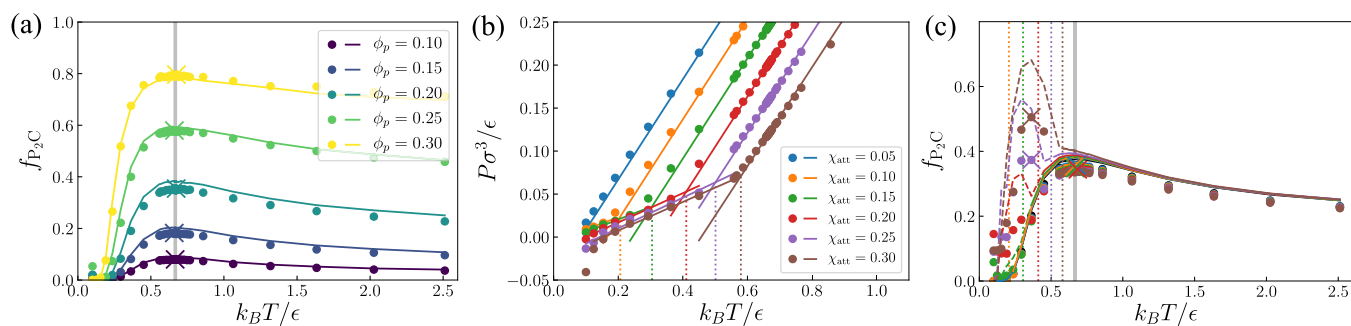
Figure 2. Effects of short-range attraction. (a) f_{P_2C} as a function of temperature k_BT/ϵ for various ϕ_p at $\chi_{att} = 0.1$. (b,c) f_{P_2C} and pressure $P\sigma^3/\epsilon$ as a function of temperature k_BT/ϵ for different short-range attraction χ_{att}. (b) Symbols are from simulations, the lines are linear fits in the two different phases, and the position of turning points, critical temperature T_c, are indicated by dotted vertical lines. (c) Dashed and solid curves are the theoretical prediction of eq 6 above and below the critical temperature T_c, respectively, with the measured K_2/K_1 from simulations. The dotted vertical lines indicate T_c measured in (b). Here $N_{poly} = 100$, $\phi_p = 0.20$, $\gamma = 2.0$, $\beta\mu_B = -2$, $\beta\mu_C = -4$, and $\beta\mu_D = -5$.
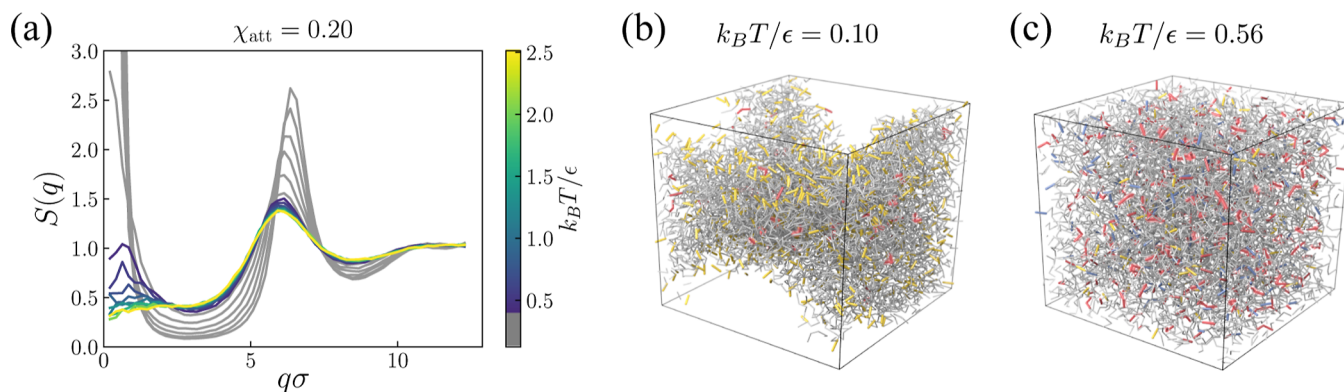
Figure 3. Structural change with decreasing temperature. (a) Structure factor $S(q)$ for systems at different temperatures, where the curves below T_c are grey. (b,c) Simulation snapshots for systems with (b) $k_BT/\epsilon = 0.10$ and (c) $k_BT/\epsilon = 0.56$. Different colors represent different types of bonds based on Figure 1c, that is, P, PC/P$_2$C, PD, and polymer backbone bonds are in blue, red, yellow, and gray, respectively. Here $N_{poly} = 100$, $\phi_p = 0.20$, $\gamma = 2.0$, $\beta\mu_B = -2$, $\beta\mu_C = -4$, and $\beta\mu_D = -5$.

monotonic behavior of f_{P_2C} with increasing T. The optimal temperature T^*, where f_{P_2C} reaches the maximum, can be obtained by solving $\partial f_{P_2C}/\partial\beta = 0$ equivalent to $\partial\Gamma/\partial\beta = 0$, which is

$$k_BT^* = \frac{-\gamma\epsilon}{\log(\gamma - 1) + \beta(\mu_D - \mu_B)} \qquad (15)$$

T^* is a positive number when $1 < \gamma < 1 + \exp[\beta(\mu_B - \mu_D)]$. When $\gamma > 1 + \exp[\beta(\mu_B - \mu_D)]$, the protecting effect of PD bonds is too strong, and f_{P_2C} increases monotonically with increasing temperature. As shown in Figure 1e, the theoretically predicted T^* agrees quantitatively with computer simulations. Intriguingly, eq 15 does not need any input from simulation or experiments, and one can also see that the optimal temperature T^* does not depend on the backbone packing fraction ϕ_p or the crosslinker chemical potential $\beta\mu_C$, which is confirmed in our MC simulations (Figure S1a,c). However, the height of the f_{P_2C} peak does depend on $\beta\mu_C$, and it changes nonmonotonically (Figure S1c). This nonmonotonic dependence originates from an entropic effect recently found in linker-mediated vitrimers.[34,44,45] Moreover, the position and height of f_{P_2C} can be also tuned by changing the concentration of B and D molecules, that is, $\beta\mu_B$ and $\beta\mu_D$ (Figure S1b,d).

Effects of the Short-Range Attraction Between Polymers

As in realistic vitrimers, there is always some short-range van der Waals attraction between polymer backbones driving the gelation at low temperature, we investigate the system with weak attraction. In Figure 2a, we plot f_{P_2C} as a function of k_BT/ϵ for systems at $\chi_{att} = 0.1$ of various polymer packing fraction $\phi_p = 0.1$ to 0.3 and $\gamma = 2$. One can see that similar to the system without attraction, with increasing temperature, f_{P_2C} first increases and then decreases to approach a plateau at high temperature, and the results from computer simulation agree quantitatively with the theoretical prediction (eq 6). We further simulate the vitrimer system by changing χ_{att} at $\phi_p = 0.2$ and $\gamma = 2$, and the results are shown in Figure 2c. At high temperatures, the simulation results agree very well with theoretical prediction, while below a certain temperature, T_c, the discrepancy appears. To understand the cause of the discrepancy, we plot the corresponding pressure $P\sigma^2/\epsilon$ as a function of temperature in the upper panel of Figure 2b. We see that with decreasing temperature, the slope of the $P - T$ curve has a turning point coinciding with the temperature threshold T_c (as indicated by the dotted vertical lines), below which the difference between simulation and theory appears. As the slope change in the $P - T$ curve normally suggests a phase separation, we plot the structure factor of the system with χ_{att} at various temperatures in Figures 3a and S2. One can see that below T_c, $S(q)$ diverges at small q, which is a signature
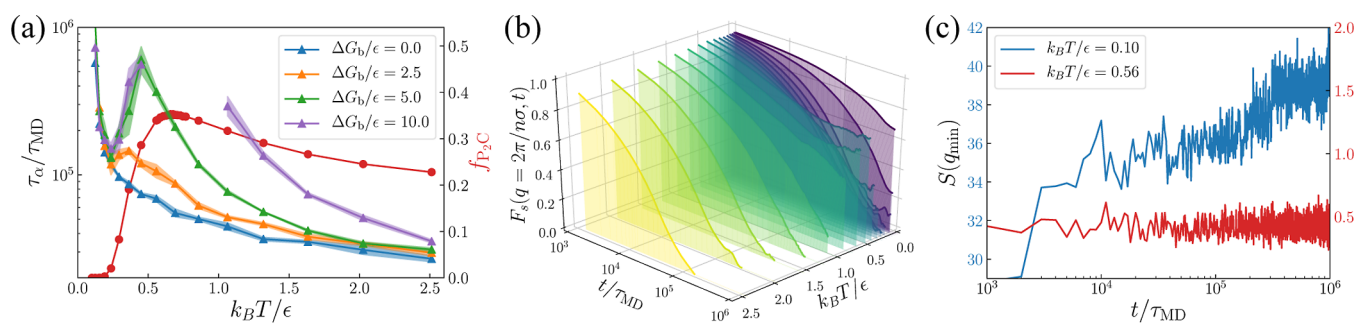
Figure 4. Thermo-gelling vitrimers. (a) Structural relaxation time, τ_α, (left) and crosslinking degree, f_{P_2C}, (right) as a function of temperature k_BT/ε for various activation barriers, ΔG_b. We note that f_{P_2C} does not depend on ΔG_b. (b) Intermediate scattering function $F_s(q, t)$ with $q = 2\pi/n\sigma$ at various temperatures k_BT/ε with $\Delta G_b/\varepsilon = 10.0$. (c) Structure factor $S(q_{min})$ with $q_{min} = 2\pi/V^{1/3}$ as a function of t at different temperatures. Here $\phi_P = 0.20$, $\gamma = 2.0$, and $\chi_{att} = 0.1$ with N_B, N_C, and N_D, obtained from MC simulations with $\beta\mu_B = -2$, $\beta\mu_C = -4$, and $\beta\mu_D = -5$.

of phase separation. This can be also seen in the snapshots of the system at different temperatures, and as shown in Figure 3b,c, when the temperature drops below $0.5\varepsilon/k_B$, for example, $k_BT/\varepsilon = 0.1$ in Figure 3b, the short-range attraction induced phase separation occurs creating interfaces, which is different from the homogeneous structure at high temperature, for example, $k_BT/\varepsilon = 0.56$ in Figure 3c. This suggests that the discrepancy between the theoretical prediction and computer simulations at low temperatures is due to the attraction-induced phase separation, which creates interfaces in the system. Although in the thermodynamic limit, the interfacial free energy is negligible, in practice, polymer systems can hardly reach a fully phase-separated equilibrium state, and this makes the free energy in eq 3 not able to correctly model the system.

Thermo-Gelling Vitrimers

Next, we perform molecular dynamics (MD) simulations to investigate the thermo-induced gelation of vitrimers. We assume all metathesis reactions share the same activation barrier ΔG_b and the rate of reaction $k = \nu_0 \exp(-\beta[\Delta G_b + \max\Delta G, 0])$, with ΔG being the reaction free energy. $\nu_0 = 1/\tau_{MD}$ is the kinetic prefactor. The activation barrier ΔG_b does not change any thermodynamic property of the system, while it does control the dynamic properties.[39] We perform hybrid event-driven molecular dynamics—Monte Carlo (EDMD-MC) NVT simulations for a system with $\phi_p = 0.2$, $\gamma = 2.0$, and $\chi_{att} = 0.1$ at different temperature starting from equilibrated configurations from grand canonical MC simulations. We plot the structural relaxation time τ_α as a function of temperature in comparison with the corresponding f_{P_2C} in Figure 4a, which is defined as $F_s(q, \tau_\alpha) = e^{-1}$, with $F_s(\cdot)$ being the intermediate scattering function. Here the diffusion is mainly through the reptation of polymer chains, so we choose $q = 2\pi/(n\sigma)$. One can see that when $\Delta G_b = 0$, τ_α decreases monotonically with increasing temperature, despite the increased crosslinking degree, f_{P_2C}. This is because increasing the temperature increases the mobility of molecules in the system, and due to the zero activation barrier of metathesis reaction, the crosslinking has minimal effects on the dynamics of the system. This is similar to the first generation vitrimer, which is a liquid at high temperature although fully crosslinked.[27] With increasing ΔG_b, the effect of crosslinking on the dynamics of the system becomes more pronounced, and τ_α starts to increase with temperature at about $0.3\varepsilon/k_B$ to develop a peak, where f_{P_2C} starts to increase as shown in Figure

4a. When $\Delta G_b = 10\varepsilon$, τ_α diverges between $k_BT/\varepsilon = 0.5$ and 1.0, and the corresponding $F_s(q, t)$ are shown in Figure 4b, which develops a plateau at both $k_BT/\varepsilon \leq 0.1$ and $0.5 < k_BT/\varepsilon < 1$. This implies that the system becomes a gel at both low and high temperatures. To distinguish the property of gels formed at different temperatures, we plot the time evolution of $S(q_{min})$ in Figure 4c, which shows the large-scale structural change in the system. One can see that at the low temperature, that is, $k_BT/\varepsilon = 0.1$, $S(q_{min})$ increases significantly with time suggesting a system that is undergoing a kinetically arrested phase separation with a very small amount of PC/P$_2$C bonds (Figure 3b), which is a typical signature of gelation induced by short-range attraction.[46] However, as shown in Figure 4c, in a high-temperature gel, that is, $k_BT/\varepsilon = 0.56$, $S(q_{min})$ does not change with time, which suggests that there is no structural change in the system, and the thermo-gelling vitrimer is an equilibrium homogeneous gel (Figure 3c) that is not subject to any thermodynamic instability.[47,48]

■ DISCUSSION AND CONCLUSIONS

In conclusion, we have proposed a novel thermo-gelling vitrimer in which, at low temperatures, the crosslinking is prevented by the protector, that is, D molecules, and with the increasing temperature, the entropy-driven crosslinking occurs, which drives the gelation of the system. We formulate a mean-field theory to describe the crosslinking, which agrees quantitatively with coarse-grained computer simulations above the gas–liquid phase separation temperature induced by the short-range van der Waals attraction in the system. Further molecular dynamics simulations show that the activation barrier of the metathesis reaction plays a crucial role during the thermo-gelling process, and it can be controlled by using different catalysts experimentally. Moreover, we show that the resulting thermo-induced gelation is an equilibrium gel not subject to any thermodynamic instability. Similar thermo-gelling systems were studied previously in patchy colloidal systems[49] and DNA nanostars,[14] and the effect was also exploited in other soft matter systems involving valency by adding corresponding protector molecules, for example, the DNA or metal coordination-mediated nanocrystals[45,50] and polyacrylamide-based hydrogels.[51] The difference is that the designed vitrimers here are covalently crosslinked, which is essentially a thermo-crosslinking elastomer. Because of the nature of metathesis reactions in vitrimers, the activation barrier can be tuned using catalysts to realize the equilibrium gel with increasing temperature, and this is qualitatively

different from conventional gelations induced by short-ranged attraction, which are essentially kinetically arrested phase separations.[46] Moreover, at high temperatures, different from the thermo-gelling systems using weak interactions, for example, hydrogen bonds, our designed vitrimers are always crosslinked because of entropy, and mechanical properties can be tuned reversibly *in situ* by changing the activation barrier using catalysts and/or adjusting the concentration of B and D molecules, which is the novelty of our designed vitrimers. The concept of vitrimers is a versatile tool that is applicable to nearly all types of polymers. Therefore, by adopting an appropriate polymer system, the thermo-gelling vitrimer designed here should be promising for biomedical applications. For example, based on the designed scheme, one could employ biocompatible silyl ether metathesis to fabricate thermo-responsive biomaterials for tissue repair and injectable implants in noninvasive surgeries.[28,52]

■ ASSOCIATED CONTENT

Ⓢ Supporting Information

The Supporting Information is available free of charge at https://pubs.acs.org/doi/10.1021/jacsau.2c00425.

> Mean-field theory for thermo-crosslinking vitrimers; chemical equilibrium and reaction equilibrium; mean-field theory at the high- and low-temperature limits; tuning thermo-crosslinking by various parameters; structure factor; and additional double bond-swap reactions (PDF)

■ AUTHOR INFORMATION

Corresponding Author

Ran Ni − *School of Chemistry, Chemical Engineering and Biotechnology, Nanyang Technological University, Singapore 637459, Singapore;* ⓞ orcid.org/0000-0001-9478-0674; Email: r.ni@ntu.edu.sg

Authors

Xiuyang Xia − *School of Chemistry, Chemical Engineering and Biotechnology, Nanyang Technological University, Singapore 637459, Singapore; Division of Physics and Applied Physics, School of Physical and Mathematical Sciences, Nanyang Technological University, Singapore 637371, Singapore;* ⓞ orcid.org/0000-0002-4851-4057

Peilin Rao − *School of Chemistry, Chemical Engineering and Biotechnology, Nanyang Technological University, Singapore 637459, Singapore;* ⓞ orcid.org/0000-0002-6973-6978

Juan Yang − *Department of Chemistry, National University of Singapore, Singapore 117546, Singapore*

Massimo Pica Ciamarra − *Division of Physics and Applied Physics, School of Physical and Mathematical Sciences, Nanyang Technological University, Singapore 637371, Singapore;* ⓞ orcid.org/0000-0001-8931-9058

Complete contact information is available at:
https://pubs.acs.org/10.1021/jacsau.2c00425

Author Contributions

R.N. conceived the research; X.X. formulated the mean-field theory and performed the Monte Carlo simulations; P. R. performed the molecular dynamics simulations; all authors discussed the results and wrote the manuscript. X.X. and P.R. contributed equally. CRediT: **Xiuyang Xia** investigation, validation, visualization, writing-original draft, writing-review & editing; **Peilin Rao** investigation, validation, visualization, writing-original draft, writing-review & editing; **Juan Yang** writing-review & editing; **Massimo Pica Ciamarra** writing-review & editing; **Ran Ni** conceptualization, funding acquisition, project administration, supervision, writing-original draft, writing-review & editing.

Notes

The authors declare no competing financial interest.
Data and materials availability: All data needed to evaluate the conclusions in the paper are presented in the paper and/or the Supporting Information. Additional data related to this paper may be requested from the authors.

■ REFERENCES

(1) Roy, D.; Brooks, W. L. A.; Sumerlin, B. S. New directions in thermoresponsive polymers. *Chem. Soc. Rev.* **2013**, *42*, 7214−7243.

(2) de las Heras Alarcón, C.; Pennadam, S.; Alexander, C. Stimuli responsive polymers for biomedical applications. *Chem. Soc. Rev.* **2005**, *34*, 276−285.

(3) Qiao, S.; Wang, H. Temperature-responsive polymers: Synthesis, properties, and biomedical applications. *Nano Res.* **2018**, *11*, 5400−5423.

(4) Dou, Q. Q.; Liow, S. S.; Ye, E.; Lakshminarayanan, R.; Loh, X. J. Biodegradable Thermogelling Polymers: Working Towards Clinical Applications. *Adv. Healthcare Mater.* **2014**, *3*, 977−988.

(5) Lendlein, A.; Langer, R. Biodegradable, Elastic Shape-Memory Polymers for Potential Biomedical Applications. *Science* **2002**, *296*, 1673−1676.

(6) Bajpai, A. K.; Shukla, S. K.; Bhanu, S.; Kankane, S. Responsive polymers in controlled drug delivery. *Prog. Polym. Sci.* **2008**, *33*, 1088−1118.

(7) Nath, N.; Chilkoti, A. Creating "Smart" Surfaces Using Stimuli Responsive Polymers. *Adv. Mater.* **2002**, *14*, 1243−1247.

(8) Chen, W.; Qu, L.; Chang, D.; Dai, L.; Ganguli, S.; Roy, A. Vertically-aligned carbon nanotubes infiltrated with temperature-responsive polymers: smart nanocomposite films for self-cleaning and controlled release. *Chem. Commun.* **2008**, 163−165.

(9) Laloyaux, X.; Fautré, E.; Blin, T.; Purohit, V.; Leprince, J.; Jouenne, T.; Jonas, A. M.; Glinel, K. Temperature-Responsive Polymer Brushes Switching from Bactericidal to Cell-Repellent. *Adv. Mater.* **2010**, *22*, 5024−5028.

(10) Hoffman, A. S.; Stayton, P. S. Conjugates of stimuli-responsive polymers and proteins. *Prog. Polym. Sci.* **2007**, *32*, 922−932.

(11) Shamim, N.; Hong, L.; Hidajat, K.; Uddin, M. S. Thermosensitive polymer coated nanomagnetic particles for separation of bio-molecules. *Sep. Purif. Technol.* **2007**, *53*, 164−170.

(12) Fujishige, S.; Kubota, K.; Ando, I. Phase transition of aqueous solutions of poly(N-isopropylacrylamide) and poly(N-isopropylmethacrylamide). *J. Phys. Chem.* **1989**, *93*, 3311−3313.

(13) Huglin, M. B.; Radwan, M. A. Unperturbed dimensions of a zwitterionic polymethacrylate. *Polym. Int.* **1991**, *26*, 97−104.

(14) Bomboi, F.; Romano, F.; Leo, M.; Fernandez-Castanon, J.; Cerbino, R.; Bellini, T.; Bordi, F.; Filetici, P.; Sciortino, F. Re-entrant DNA gels. *Nat. Commun.* **2016**, *7*, 13191.

(15) Kapnistos, M.; Vlassopoulos, D.; Fytas, G.; Mortensen, K.; Fleischer, G.; Roovers, J. Reversible Thermal Gelation in Soft Spheres. *Phys. Rev. Lett.* **2000**, *85*, 4072−4075.

(16) Zhang, H.; Yu, L.; Ding, J. Roles of Hydrophilic Homopolymers on the Hydrophobic-Association-Induced Physical Gelling of Amphiphilic Block Copolymers in Water. *Macromolecules* **2008**, *41*, 6493−6499.

(17) Moon, H. J.; Ko, D. Y.; Park, M. H.; Joo, M. K.; Jeong, B. Temperature-responsive compounds as in situ gelling biomedical materials. *Chem. Soc. Rev.* **2012**, *41*, 4860−4883.

(18) Yuan, M.; Bi, B.; Huang, J.; Zhuo, R.; Jiang, X. Thermosensitive and photocrosslinkable hydroxypropyl chitin-based hydrogels for biomedical applications. *Carbohydr. Polym.* **2018**, *192*, 10−18.

(19) Dong, Y.; Hassan, W.; Zheng, Y.; Saeed, A. O.; Cao, H.; Tai, H.; Pandit, A.; Wang, W. Thermoresponsive hyperbranched copolymer with multi acrylate functionality for in situ cross-linkable hyaluronic acid composite semi-IPN hydrogel. *J. Mater. Sci. Mater. Med.* **2012**, *23*, 25−35.

(20) van de Wetering, P.; Metters, A. T.; Schoenmakers, R. G.; Hubbell, J. A. Poly(ethylene glycol) hydrogels formed by conjugate addition with controllable swelling, degradation, and release of pharmaceutically active proteins. *J. Controlled Release* **2005**, *102*, 619−627.

(21) Sakai, S.; Hirose, K.; Moriyama, K.; Kawakami, K. Control of cellular adhesiveness in an alginate-based hydrogel by varying peroxidase and H2O2 concentrations during gelation. *Acta Biomater.* **2010**, *6*, 1446−1452.

(22) Lee, F.; Chung, J. E.; Kurisawa, M. An injectable hyaluronic acid-tyramine hydrogel system for protein delivery. *J. Controlled Release* **2009**, *134*, 186−193.

(23) Vermonden, T.; Fedorovich, N. E.; van Geemen, D.; Alblas, J.; van Nostrum, C. F.; Dhert, W. J. A.; Hennink, W. E. Photo-polymerized Thermosensitive Hydrogels: Synthesis, Degradation, and Cytocompatibility. *Biomacromolecules* **2008**, *9*, 919−926.

(24) Lee, S. H.; Lee, Y.; Lee, S. W.; Ji, H.-Y.; Lee, J.-H.; Lee, D. S.; Park, T. G. Enzyme-mediated cross-linking of Pluronic copolymer micelles for injectable and in situ forming hydrogels. *Acta Biomater.* **2011**, *7*, 1468.

(25) Nezhad-Mokhtari, P.; Ghorbani, M.; Roshangar, L.; Soleimani Rad, J. S. Chemical gelling of hydrogels-based biological macro-molecules for tissue engineering: Photo- and enzymatic-crosslinking methods. *Int. J. Biol. Macromol.* **2019**, *139*, 760.

(26) Cellesi, F.; Tirelli, N.; Hubbell, J. A. Materials for Cell Encapsulation via a New Tandem Approach Combining Reverse Thermal Gelation and Covalent Crosslinking. *Macromol. Chem. Phys.* **2002**, *203*, 1466.

(27) Montarnal, D.; Capelot, M.; Tournilhac, F.; Leibler, L. Silica-like malleable materials from permanent organic networks. *Science* **2011**, *334*, 965−968.

(28) Tretbar, C. A.; Neal, J. A.; Guan, Z. Direct Silyl Ether Metathesis for Vitrimers with Exceptional Thermal Stability. *J. Am. Chem. Soc.* **2019**, *141*, 16595−16599.

(29) Wu, D.-C.; Loh, X. J.; Wu, Y.-L.; Lay, C. L.; Liu, Y. 'Living' Controlled in Situ Gelling Systems: Thiol−Disulfide Exchange Method toward Tailor-Made Biodegradable Hydrogels. *J. Am. Chem. Soc.* **2010**, *132*, 15140−15143.

(30) Pepels, M.; Filot, I.; Klumperman, B.; Goossens, H. Self-healing systems based on disulfide-thiol exchange reactions. *Polym. Chem.* **2013**, *4*, 4955−4965.

(31) Cho, I. S.; Ooya, T. An injectable and self-healing hydrogel for spatiotemporal protein release via fragmentation after passing through needles. *J. Biomater. Sci. Polym. Ed.* **2018**, *29*, 145−159.

(32) Jiang, L.; Tian, Y.; Cheng, J.; Zhang, J. A biomass-based Schiff base vitrimer with both excellent performance and multiple degradability. *Polym. Chem.* **2021**, *12*, 6527−6537.

(33) Röttger, M.; Domenech, T.; van der Weegen, R.; Breuillac, A.; Nicolaÿ, R.; Leibler, L. High-performance vitrimers from commodity thermoplastics through dioxaborolane metathesis. *Science* **2017**, *356*, 62−65.

(34) Lei, Q. L.; Xia, X.; Yang, J.; Pica Ciamarra, M. P.; Ni, R. Entropy-controlled cross-linking in linker-mediated vitrimers. *Proc. Natl. Acad. Sci. U.S.A.* **2020**, *117*, 27111−27115.

(35) Weeks, J. D.; Chandler, D.; Andersen, H. C. Role of repulsive forces in determining the equilibrium structure of simple liquids. *J. Chem. Phys.* **1971**, *54*, 5237−5247.

(36) Hansen, J.-P.; McDonald, I. R. *Theory of Simple Liquids*; Elsevier, 1990; pp 94−96.

(37) Bernard, E. P.; Krauth, W.; Wilson, D. B. Event-chain Monte Carlo algorithms for hard-sphere systems. *Phys. Rev. E: Stat., Nonlinear, Soft Matter Phys* **2009**, *80*, 056704.

(38) Kampmann, T. A.; Boltz, H.-H.; Kierfeld, J. Monte Carlo simulation of dense polymer melts using event chain algorithms. *J. Chem. Phys.* **2015**, *143*, 044105.

(39) Wu, J.-B.; Li, S.-J.; Liu, H.; Qian, H.-J.; Lu, Z.-Y. Dynamics and reaction kinetics of coarse-grained bulk vitrimers: A molecular dynamics study. *Phys. Chem. Chem. Phys.* **2019**, *21*, 13258−13267.

(40) Stukalin, E. B.; Cai, L.-H.; Kumar, N. A.; Leibler, L.; Rubinstein, M. Self-healing of unentangled polymer networks with reversible bonds. *Macromolecules* **2013**, *46*, 7525−7541.

(41) Hoy, R. S.; Fredrickson, G. H. Thermoreversible associating polymer networks. I. Interplay of thermodynamics, chemical kinetics, and polymer physics. *J. Chem. Phys.* **2009**, *131*, 224902.

(42) Frenkel, D.; Smit, B. *Understanding Molecular Simulation: From Algorithms to Applications*; Elsevier, 2001; Vol. *1*, pp 141−146.

(43) Andersen, H. C. Molecular dynamics simulations at constant pressure and/or temperature. *J. Chem. Phys.* **1980**, *72*, 2384−2393.

(44) Wu, S.; Yang, H.; Huang, S.; Chen, Q. Relationship between Reaction Kinetics and Chain Dynamics of Vitrimers Based on Dioxaborolane Metathesis. *Macromolecules* **2020**, *53*, 1180−1190.

(45) Xia, X.; Hu, H.; Ciamarra, M. P.; Ni, R. Linker-mediated self-assembly of mobile DNA-coated colloids. *Sci. Adv.* **2020**, *6*, No. eaaz6921.

(46) Lu, P. J.; Zaccarelli, E.; Ciulla, F.; Schofield, A. B.; Sciortino, F.; Weitz, D. A. Gelation of particles with short-range attraction. *Nature* **2008**, *453*, 499−503.

(47) Sciortino, F.; Zaccarelli, E. Equilibrium gels of limited valence colloids. *Curr. Opin. Colloid Interface Sci.* **2017**, *30*, 90−96.

(48) Hurtado, P. I.; Berthier, L.; Kob, W. Heterogeneous Diffusion in a Reversible Gel. *Phys. Rev. Lett.* **2007**, *98*, 135503.

(49) Roldán-Vargas, S.; Smallenburg, F.; Kob, W.; Sciortino, F. Gelling by heating. *Sci. Rep.* **2013**, *3*, 1−5.

(50) Kang, J.; Valenzuela, S. A.; Lin, E. Y.; Dominguez, M. N.; Sherman, Z. M.; Truskett, T. M.; Anslyn, E. V.; Milliron, D. J. Colorimetric quantification of linking in thermoreversible nanocrystal gel assemblies. *Sci. Adv.* **2022**, *8*, No. eabm7364.

(51) FitzSimons, T. M.; Anslyn, E. V.; Rosales, A. M. Effect of pH on the Properties of Hydrogels Cross-Linked via Dynamic Thia-Michael Addition Bonds. *ACS Polym. Au* **2021**, *2*, 129−136.

(52) Parrott, M. C.; Luft, J. C.; Byrne, J. D.; Fain, J. H.; Napier, M. E.; DeSimone, J. M. Tunable Bifunctional Silyl Ether Cross-Linkers for the Design of Acid-Sensitive Biomaterials. *J. Am. Chem. Soc.* **2010**, *132*, 17928−17932.